

Photoactivatable Odorants for Chemosensory Research

Sangram Gore,[¶] Kirill Ukhanov,[¶] Cyril Herbivo, Naeem Asad, Yuriy V. Bobkov, Jeffrey R. Martens,* and Timothy M. Dore*Cite This: <https://dx.doi.org/10.1021/acscchembio.0c00541>

Read Online

ACCESS |



Metrics & More

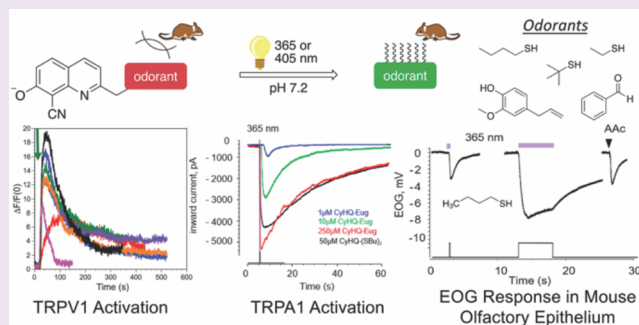


Article Recommendations



Supporting Information

ABSTRACT: The chemosensory system of any animal relies on a vast array of detectors tuned to distinct chemical cues. Odorant receptors and the ion channels of the TRP family are all uniquely expressed in olfactory tissues in a species-specific manner. Great effort has been made to characterize the molecular and pharmacological properties of these proteins. Nevertheless, most of the natural ligands are highly hydrophobic molecules that are not amenable to controlled delivery. We sought to develop photoreleasable, biologically inactive odorants that could be delivered to the target receptor or ion channel and effectively activated by a short light pulse. Chemically distinct ligands eugenol, benzaldehyde, 2-phenethylamine, ethanethiol, butane-1-thiol, and 2,2-dimethylethane-1-thiol were modified by covalently attaching the photoremovable protecting group (8-cyano-7-hydroxyquinolin-2-yl)methyl (CyHQ). The CyHQ derivatives were shown to release the active odorant upon illumination with 365 and 405 nm light. We characterized their bioactivity by measuring activation of recombinant TRPV1 and TRPA1 ion channels expressed in HEK 293 cells and the electroolfactogram (EOG) response from intact mouse olfactory epithelium (OE). Illumination with 405 nm light was sufficient to robustly activate TRP channels within milliseconds of the light pulse. Photoactivation of channels was superior to activation by conventional bath application of the ligands. Photolysis of the CyHQ-protected odorants efficiently activated an EOG response in a dose-dependent manner with kinetics similar to that evoked by the vaporized odorant amyl acetate (AAc). We conclude that CyHQ-based, photoreleasable odorants can be successfully implemented in chemosensory research.



INTRODUCTION

The olfactory system has a central function in the detection and interpretation of chemical cues present in the environment.^{1–4} Odorants are low molecular weight volatile compounds that can be detected by the human or animal olfactory system. In all living organisms, odorants play important roles, particularly in environmental threat detection,^{5,6} food scavenging,⁷ disease detection,^{8,9} navigation,^{10,11} mate recognition,^{12,13} and appetite stimulation.^{14–16} In terrestrial vertebrates, odorants are inhaled into the nasal cavity where they are recognized by olfactory sensory neurons (OSNs) in the olfactory epithelium (OE). Odorant binding to the receptors on these neurons activates signaling pathways in a ligand-dependent manner that transmit information directly to glomeruli in the olfactory bulb and further to the brain, where odor perception is constructed.^{17,18}

There are about 400 human and more than 1000 mouse genes that encode olfactory receptors (ORs), which comprise one of the largest families of G-protein coupled receptors (GPCRs).^{19,20} ORs along with ion channels of the transient receptor potential (TRP) family are uniquely expressed in a tissue-specific manner. As one of the most significant elements in smell sensory neurons, ORs greatly contribute to a high performance olfactory system that can identify various odor

molecules from different chemical classes, such as ketones, carboxylic acids, alcohols, aldehydes, sulfur-containing compounds, and others.^{21,22} One OR recognizes multiple odorants, and one odorant is recognized by multiple ORs, and interestingly, different odorants are recognized by different combinations of ORs.²³ Most of the natural ligands are highly hydrophobic molecules that are difficult to deliver to the immediate vicinity of the ORs in native tissue, which is important for high resolution imaging and study of the signaling pathways. The process of olfactory transduction takes place at the fine cilia, which makes the experimental manipulations for studying olfactory receptors difficult.

To address this challenge, we designed and synthesized photoactivatable odorants that can be delivered to the target receptor or ion channel in intact olfactory tissues and effectively activated by a brief light pulse to enable the study of this chemosensory system. We used (8-cyano-7-hydrox-

Received: July 6, 2020

Accepted: August 14, 2020



quinolin-2-yl)methyl (CyHQ)^{24–27} as the photoremovable protecting group (PPG) to inactivate the odorants because of its excellent photochemical properties and biocompatibility, such as good solubility in aqueous media, high quantum yields, and fast release kinetics in a clean reaction that releases the attached biological effectors in high yield along with biologically benign byproducts. We prepared CyHQ-protected versions of the odorants benzaldehyde (CyHQ-BZA), 2-phenethylamine (CyHQ-2PEA), eugenol (CyHQ-EG), ethanethiol (CyHQ-(SEt)₂), butane-1-thiol (CyHQ-(SBu)₂), and 2,2-dimethylethane-1-thiol (CyHQ-(St-Bu)₂) (Figure 1). A

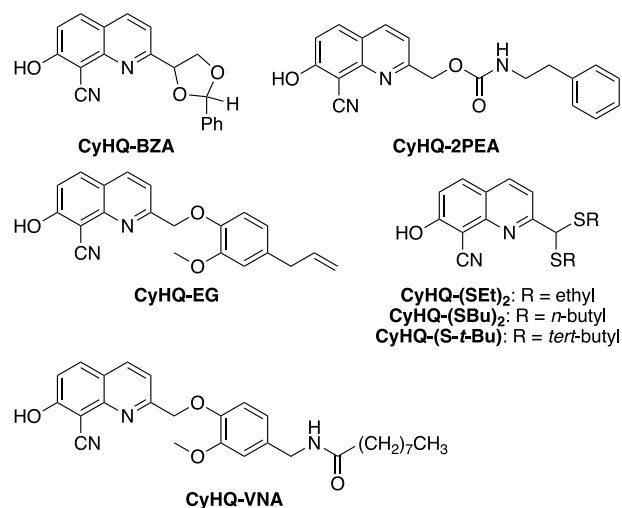


Figure 1. CyHQ-protected odorants and CyHQ-VNA.

photoactivatable form of the equipotent capsaicin analogue *N*-(4-hydroxy-3-methoxybenzyl)nonanamide (VNA),²⁸ which activates TRPV1 channels,^{29–32} CyHQ-VNA,²⁵ was used as a positive control to evaluate the odorants' ability to activate TRPV1 channels.³³ Other photoactivatable forms of capsaicin³³ or VNA^{34–37} exist, but none have the high sensitivity and rapid capsaicinoid release kinetics of CyHQ-VNA. The CyHQ-protected odorants were evaluated for their ability to activate TRPA1 channels and induce a dose-dependent electroolfactogram (EOG) in native mouse OE.

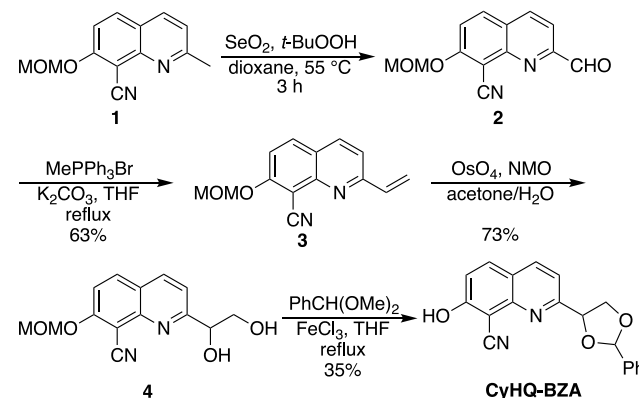
RESULTS AND DISCUSSION

Design. Creation of the CyHQ-protected versions of the odorants required the development of some new photochemistry. The design of CyHQ-BZA was inspired by previous work that identified a bromohydroxycoumarin derivative, Bhcdiol,³⁸ as a PPG suitable for mediating the photorelease of ketones and aldehydes. Because primary amines are not sufficiently good leaving groups, a carbamate linkage was used to prepare CyHQ-2PEA. CyHQ-EG was designed based on previous work that showed that quinoline-derived PPGs effectively mediated the release of phenols under physiological conditions.^{25,39} Directly releasing alkanethiols from PPGs is challenging because the photochemistry often generates sulfur-based radicals that react with the PPG and other species in the system. Nevertheless, some creative solutions to the problem have been reported.^{40–46} Quinoline-based PPGs do not release thiols directly from the thioether. To overcome this, we were inspired by the ability of the (8-bromo-7-hydroxyquinolin-2-yl)methyl (BHQ) PPG to release diols.⁴⁷ Our design uses

CyHQ-thioacetals to mediate the photoactivation of alkanethiols.

Synthesis. CyHQ-BZA was prepared from the previously reported aldehyde **2**,²⁴ which we synthesized from **1** using an improved procedure (Scheme 1).²⁶ Wittig olefination provided

Scheme 1. Preparation of CyHQ-Protected Benzaldehyde



alkene **3**, which was oxidized by osmium(VIII) oxide to diol **4** in 73% yield. The reaction of **4** with (dimethoxymethyl)benzene in the presence of iron(III) chloride in refluxing THF afforded CyHQ-BZA.

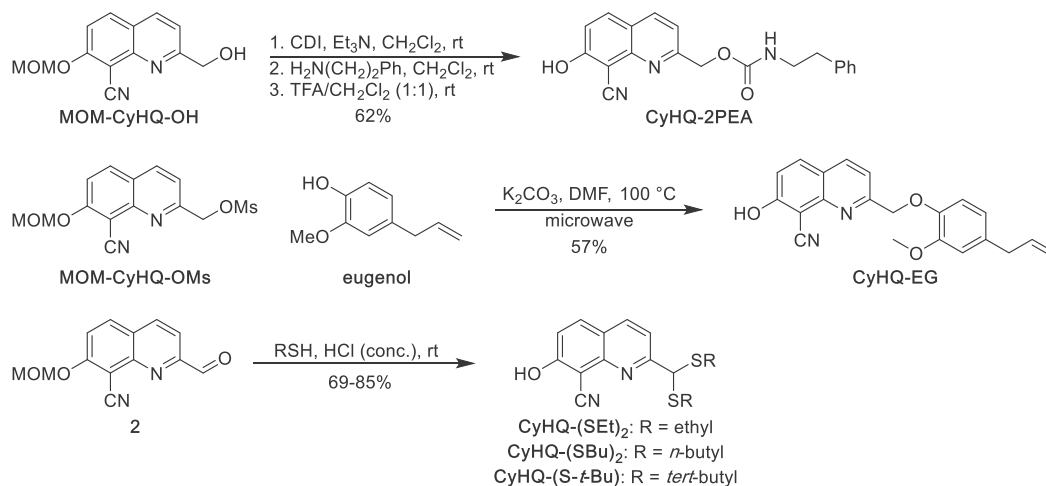
CyHQ-2PEA was prepared by first activating the primary alcohol on MOM-CyHQ-OH (prepared as previously described^{24,26}) with 1,1'-carbonyldiimidazole (CDI) followed by displacement of the remaining imidazole with phenethylamine (Scheme 2). CyHQ-EG was prepared in moderate yield by heating eugenol with MOM-CyHQ-OMs (prepared as previously described²⁶) in DMF in the presence of potassium carbonate (Scheme 2). The CyHQ-protected thiols CyHQ-(SEt)₂, CyHQ-(SBu)₂, and CyHQ-(St-Bu)₂ were synthesized in moderate to good yields from aldehyde **2** (Scheme 1) using the corresponding thiols (ethanethiol, butane-1-thiol, and 2,2-dimethylethane-1-thiol) (Scheme 2) and concentrated hydrochloric acid. CyHQ-VNA (Figure 1) was prepared as previously described.²⁵

Photochemistry. Each of the CyHQ-protected odorants photolyzed efficiently when exposed to 365 or 405 nm light under simulated physiological conditions (pH 7.2 KMOPS buffer) (Scheme 3, Figure 2, and Table 1). The 405 nm wavelength was tested because this laser line is commonly found on commercially available turn-key confocal microscope systems and can be used for photoactivation. The photochemistry of CyHQ-VNA has been reported previously.²⁵

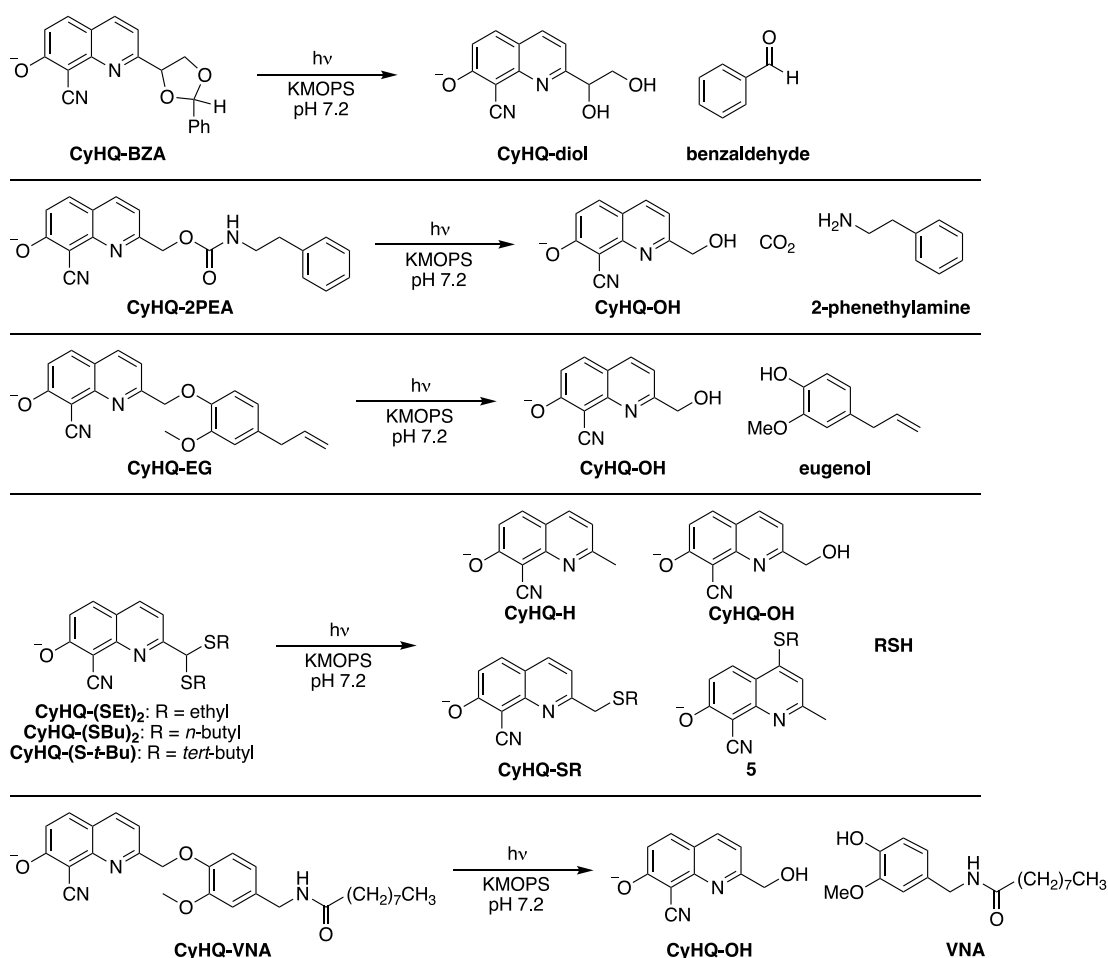
CyHQ-BZA released benzaldehyde reasonably efficiently at 365 and 405 nm light, although prolonged exposure shows significant disappearance of benzaldehyde under the reaction conditions. Benzaldehyde does not absorb light above 300 nm, so the decomposition is likely the result of nonphotochemical air oxidation to benzoic acid. CyHQ-2PEA photolyzed efficiently, resulting in a ~70% yield of 2-phenethylamine. CyHQ-EG photolyzed with moderate quantum efficiencies at 365 and 405 nm, but the yield of eugenol was much lower than expected. The expected products CyHQ-OH and eugenol were readily observed in the HPLC and LC-MS traces, but no other discrete products (e.g., isoeugenol) were detected, only nonspecific decomposition.

The photolysis of the CyHQ-protected thiols yielded a variety of quinoline-based photoproducts, including CyHQ-H,

Scheme 2. Synthesis of CyHQ-Protected 2-Phenethylamine, Eugenol, and Alkyl Thiols



Scheme 3. Photolysis Reactions of CyHQ-Protected Odorants



CyHQ-OH, CyHQ-SR, and thioether **5** (Scheme 3) in addition to the alkanethiol. Release of the alkanethiol was evident because of the distinct foul smell that emanated from the reaction vessel within seconds of light exposure and increased in intensity as the photolysis reaction progressed. Ethanethiol and 2,2-dimethylethane-1-thiol are used to tag liquid petroleum gas (LPG) and natural gas, respectively, and butane-1-thiol is used in “stink bombs”. The human olfactory system detects these odorants at 0.36, 0.33, and 1.4 ppb levels,

respectively.⁴⁸ CyHQ-(SEt)₂ and CyHQ-(SBU)₂ photolyzed with quantum efficiencies, $\Phi_u = 0.34$ (365 nm) and 0.37 (405 nm) and $\Phi_u = 0.26$ (365 nm) and 0.20 (405 nm), respectively, whereas CyHQ-(S-*t*-Bu)₂ displayed much lower quantum efficiencies.

CyHQ-BZA, CyHQ-2PEA, CyHQ-EG, CyHQ-(SEt)₂, CyHQ-(SBU)₂, CyHQ-(S-*t*-Bu)₂, and CyHQ-VNA²⁵ had sufficient solubility in the KMOPS buffer and adequate

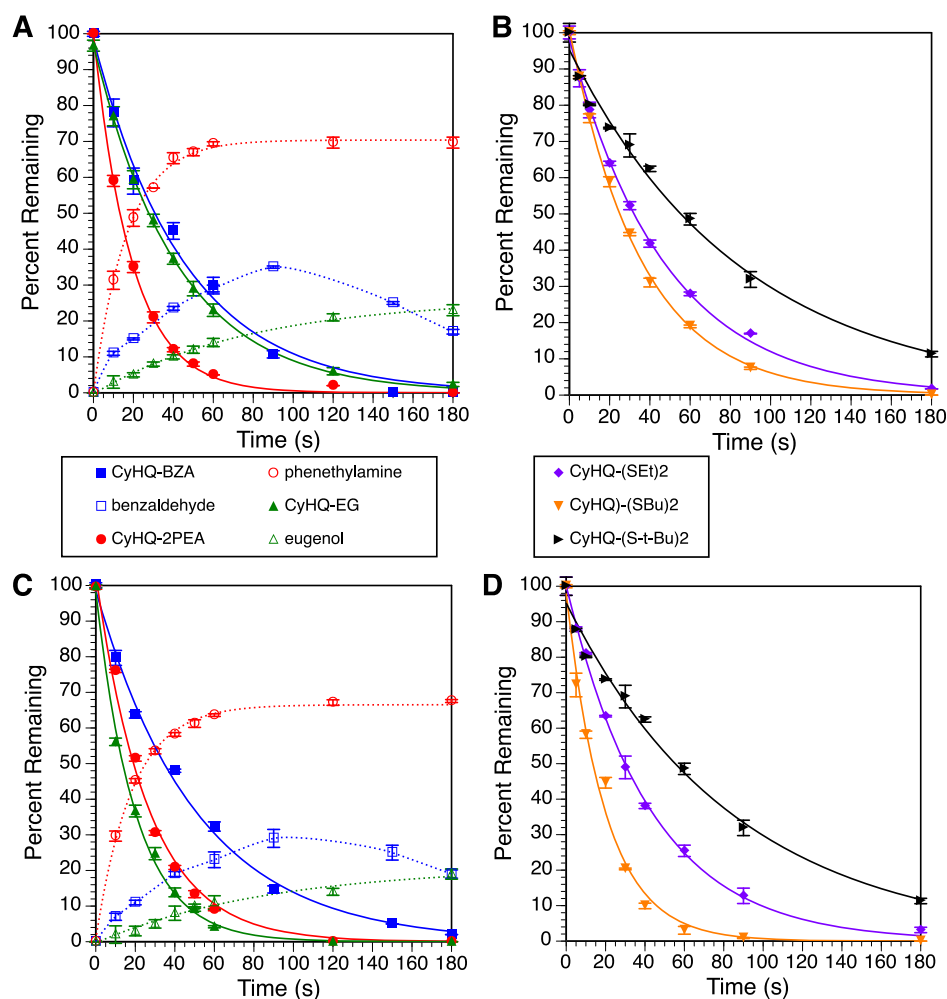


Figure 2. Time courses of the photolysis reactions at (A, B) 365 nm and (C, D) 405 nm. Percentage remaining was determined by HPLC analysis and is the average of three runs. Solid lines are least-squares fits of the data to a simple exponential decay. Dashed lines are least-squares fits of the data to an exponential rise to max or a spline curve in the case of benzaldehyde. Error bars represent the standard deviation of the mean.

Table 1. Photochemical Properties of CyHQ-Protected Odorants^a

compound	λ_{\max} (nm)	ϵ_{365} ($M^{-1} \text{ cm}^{-1}$)	ϵ_{405} ($M^{-1} \text{ cm}^{-1}$)	$\Phi_{u(365)}$	$\Phi_{u(405)}$	sensitivity ($\epsilon_{365}\Phi_u$)	sensitivity ($\epsilon_{405}\Phi_u$)	yield ^b (365 nm) (%)	yield ^b (405 nm) (%)	dark stability (h) ^c
CyHQ-BZA	365	5500	470	0.13	0.11	694	44	35	30	24
CyHQ-2PEA	365	7460	280	0.34	0.31	2487	88	70	70	48
CyHQ-EG	365	7340	798	0.21	0.15	1541	121	25	19	24
CyHQ-(SEt) ₂	368	3340	1000	0.34	0.37	1121	370			24
CyHQ-(SBu) ₂	368	5350	710	0.26	0.20	1378	140			24
CyHQ-(S-t-Bu) ₂	387	6650	6200	0.09	0.07	567	444			48
CyHQ-VNA ^d	368	6100		0.41		2501		65		100

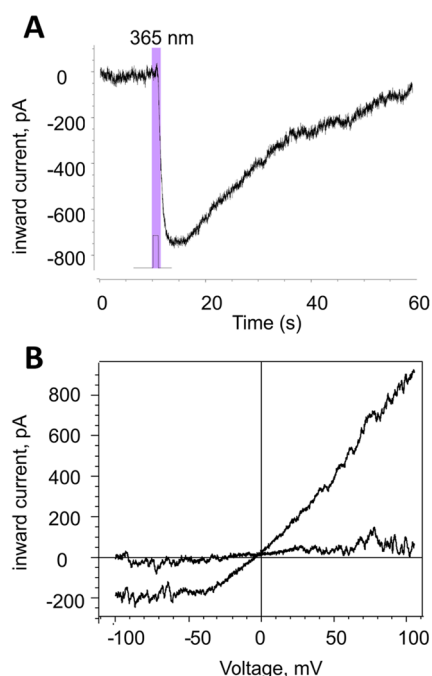
^a0.1 mM solution in KMOPS buffer, pH 7.2. ^bYield of benzaldehyde, 2-phenethylamine, or eugenol as measured by HPLC. ^cNo spontaneous hydrolysis in the dark observed within the time given. ^dData taken from the literature on CyHQ-protected *N*-(4-hydroxy-3-methoxybenzyl)-acetamide, commonly known as *N*-vanillyl-acetamide (VAA), an analogue of CyHQ-VNA that is more soluble in aqueous buffers to the extent needed for analyzing photochemical reactions.²⁵

stability toward spontaneous hydrolysis in the dark, making them fit for studies in biological systems.

Activation of TRPV1 Channels Using CyHQ-Protected Odorants and VNA. Several odorant and flavor molecules, including eugenol, have been characterized as activators of ion channels belonging to the TRP family, including TRPA1 and TRPV1.^{31,49,50} Both TRPA1 and TRPV1 channels can be activated by electrophilic pungent molecules like capsaicin,

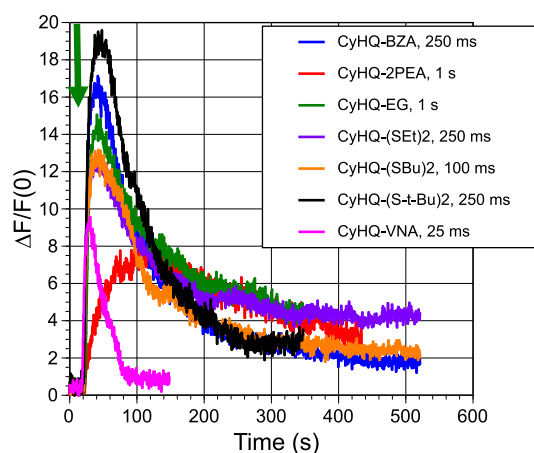
allicin, allyl isothiocyanate, and vanillin.^{51,52} Eugenol is a known odorant ligand for several mammalian and insect olfactory receptors,^{53,54} and it is unique in its anti-inflammatory potential and antibacterial activity against human pathogens.^{55,56} The CyHQ-protected odorants were tested for their ability to activate TRPV1 channels on cultured HEK 293 cells that expressed human TRPV1 on the cell membranes in comparison to CyHQ-VNA.²⁵

HEK 293 cells were transiently cotransfected with cDNA encoding human TRPV1 and GFP. Only cells visible by their green fluorescence were used for patch clamp recording. Inward ionic current was measured in a whole-cell voltage clamp configuration in a single cell superfused with either control physiological solution or supplemented with the indicated concentration of the CyHQ-protected odorant. For photolysis, we used 365 nm light to most closely match the maximum wavelength of excitation of the CyHQ-protected odorants (see Supporting Information for UV-vis spectra) and VNA. In the presence of CyHQ-VNA (10 μ M), a 100 ms pulse of 365 nm light from an LED at 50% of its maximal output robustly activated inward ionic current with a latency of 69.5 ± 10.9 ms (3 cells) and a current-voltage dependence that is typical for TRPV1 (Figure 3).⁵¹ A TRPV1-dependent ion



current was evoked multiple times in the same cell, suggesting very little inactivation. Importantly, the 475 nm light used to visualize GFP did not activate any inward current prior to the photoactivation pulse, supporting the utility of a Ca^{2+} imaging assay to perform higher throughput screening of the photoactivatable odorants. Photolysis of the CyHQ-protected odorants with 405 nm light produced active compounds (Figure 2), which suggested that photoactivation can be conveniently accomplished using a laser line that is standard for most commercially available

confocal microscopes. To demonstrate, we used 405 nm light and the CyHQ-protected odorants to activate TRPV1 channels stably expressed in cultured HEK 293 cells. Photochemical release of the capsaicinoid VNA from CyHQ-VNA²⁵ served as a positive control. The TRPV1-expressing HEK 293 cells were incubated with the Ca^{2+} sensitive dye Fluo-4 AM and the CyHQ-protected odorants or CyHQ-VNA. Using a confocal microscope, the Ca^{2+} influx into the cells was measured by imaging at 488 nm before and after a brief pulse of 405 nm light directed close to the external side of the cell membrane (Figure 4). The concentration of each CyHQ-protected



odorant and the laser power were held constant, and the duration of the light exposure varied to maximize the fluorescence signal with minimal toxicity to cells. Benzaldehyde, 2-phenethylamine, eugenol, ethanethiol, butane-1-thiol, and 2,2-dimethylethane-1-thiol were not as potent activators of the TRPV1 channel as VNA, which gave a robust response with a 25 ms pulse of 405 nm light that could be repeated to give a consistent Ca^{2+} response (Figure S8). The fluorescent signal from release of VNA from CyHQ-VNA depended on concentration and light intensity (Figure S9). Among the odorants, CyHQ-(S-Bu)₂ was the most potent because it gave a response comparable to that from CyHQ-VNA with the shortest duration of light pulse (100 ms) compared to 250 ms for CyHQ-(SEt)₂ and CyHQ-(S-t-Bu)₂. The rise times of the fluorescent signals for the CyHQ-protected odorants were slightly longer than those of CyHQ-VNA except that of CyHQ-2PEA, which was significantly longer (Table 2), indicating rapid channel opening after photolysis of most of the CyHQ-protected odorants and VNA. The delayed channel activation with CyHQ-2PEA is likely due to the fact that a slow decarboxylation step after photocleavage of the carbamate is required to reveal the active amine. The lower potency of the odorants might explain the slightly longer rise times compared to VNA. The fluorescent signal did not return to its original level prior to light exposure when the odorants were released, whereas the signal did return to baseline when the TRPV1 channels were photoactivated by

Table 2. Rise Times for Photoactivation of TRPV1 Channels after Photoactivation of CyHQ-Protected Odorants and VNA^a

compound	rise time (s)
CyHQ-BZA	7.8
CyHQ-2PEA	49.8
CyHQ-EG	8.9
CyHQ-(SEt) ₂	7.0
CyHQ-(SBU) ₂	7.8
CyHQ-(S- <i>t</i> -Bu) ₂	8.9
CyHQ-VNA	4.0

^aRise time = $t_{90\%} - t_{10\%}$, where $t_{90\%}$ and $t_{10\%}$ are the times at 90% and 10% of max response, respectively, taken from the data in Figure 4.

CyHQ-VNA. This might have resulted from saturating stimulation of the TRPV1 channels that prolonged recovery, left some channels open, or both. Further, the odorants are small and lipophilic and could have been absorbed into the membrane to create a reservoir of activator ligands that slowly released to interact with TRPV1. We confirmed that even prolonged illumination with 488 nm light used for Fluo-4 imaging was not able to activate any TRPV1-mediated Ca²⁺ influx. We conclude that CyHQ photoprotection provided excellent spectral selectivity essential to perform high-

resolution multicolor microscopy along with photorelease of odorants.

Activation of Human TRPA1 Ion Channels Using CyHQ-Protected Odorants. We tested whether CyHQ-EG could be used as a prototypic photoprotected odorant relevant for chemosensory biology. Whole-cell ionic currents were recorded from HEK 293 cells transiently coexpressing recombinant human TRPA1 channels and GFP. Bath application of eugenol, using a rapid superfusion system that enabled the solution exchange in less than 10 ms, activated an inward current following a significant delay (Figure 5A). Illumination of TRPA1-expressing cells with 365 nm light or bath application of CyHQ-EG (250 μM) alone did not activate any inward current (Figure 5A). However, following a short waiting period after the solution exchange from normal Ringer to that containing CyHQ-EG, a 100 ms pulse of 365 nm light from an LED at 50% output robustly activated inward ionic current with fast kinetics (Figure 5B). Photolysis-evoked inward current was detected with a latency of 87.8 ± 10.8 ms and a time to reach 90% of the peak magnitude of 1.7 ± 0.2 s (4 cells, $n = 5$). The inward ionic current had a current–voltage relationship typical for TRPA1 (Figure 5C).^{51,57} Because cells were superfused with the solution containing a given concentration of CyHQ-EG, we measured the concentration dependence of the TRPA1-mediated current

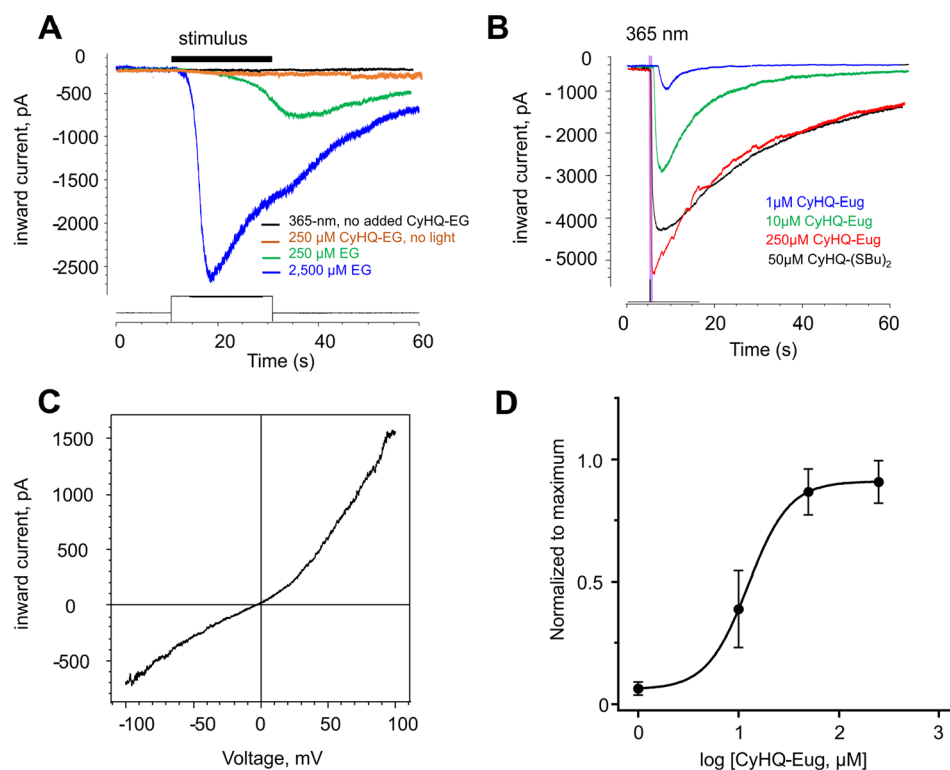


Figure 5. Photoactivation of human TRPA1 channels transiently expressed in HEK 293. (A) Prolonged 20 s illumination with 365 nm light with no added CyHQ-EG as well as application of CyHQ-EG (250 μM) in the absence of light did not activate any current. A 20 s superfusion with eugenol (250 and 2500 μM) activated ionic current with typical delayed TRPA1 kinetics. (B) A whole-cell inward current measured in a single HEK293T cell transiently expressing TRPA1 and superfused with increasing concentrations of CyHQ-EG prior to illumination with a 100 ms pulse of 365 nm light from an LED at 50% power output given at the indicated time. For comparison, photolysis of CyHQ-(SBU)₂ (50 μM) also robustly activated TRPA1. (C) A current–voltage relationship of the TRPA1 mediated current, corrected for leak current, was measured at the decaying phase. A continuous voltage ramp spanning –100 to +100 mV in 500 ms was applied to measure the current. (D) Concentration dependence of the TRPA1 current evoked by photolysis of CyHQ-EG superfused in cells at the indicated concentration and illuminating with a 100 ms pulse of 365 nm light from an LED at 50% output power. The amplitude was normalized to the maximum of the inward current in each series. Data points were fitted to a Hill equation yielding a Hill slope of 2.1 and $EC_{50} = 12.6$ μM.

evoked by light of the same intensity and duration (Figure 5D). Notably, as little as 1 μM CyHQ-EG was sufficient to photoactivate TRPA1 channels (Figure 5B). Photoprotected thiol CyHQ-(SBU)₂ (50 μM) was also an effective photoactivator of the TRPA1 channel (Figure 5B and S10). Other CyHQ-protected odorants, 2-phenethylamine (nonrelevant TRPA1 ligand) and benzaldehyde (a weak agonist with EC₅₀ > 300 μM),⁵⁸ did not photoactivate TRPA1 channels as strongly as CyHQ-(SBU)₂ (Figure S10).

One important caveat emerged from comparing the kinetics of TRPV1 and TRPA1 channel activation by bath applied odorants and by photolysis of the CyHQ-protected odorants. In our study and previously published work from other laboratories, bath applied TRPA1 and TRPV1 agonists took a relatively longer time to activate the ion channel, suggesting it takes time to diffuse to the cell from the point of introduction into the culture and interact with the channels. The binding site for capsaicinoids on TRPV1 is outside the cell,^{59–61} whereas electrophilic TRPA1 agonists covalently modify cysteine residues on the cytosolic side of the membrane,^{62,63} so odorants would have the added step of permeating the membrane before interacting with TRPA1. CyHQ-protected odorants significantly shorten the latency time relative to bath application of the odorants because they deliver the inactive odorant to the vicinity of the channel protein moiety, which makes them available for fast chemical interaction with the receptor channel upon photolysis. The CyHQ-odorant conjugates are small, relatively lipophilic molecules that cross cell membranes, similarly to many other so-called “caged” compounds, so it would be reasonable to expect that they would be present inside the HEK293 cells and facilitate short latency times for TRPA1 activation. We conclude that CyHQ-protected odorants represent a novel class of agonists enabling tight control of the dynamics of TRPA1 and TRPV1 activation.

Photoactivation of Odorants Induces Response in Mouse Olfactory Epithelium. To test if CyHQ-protected odorants can activate native sensory neurons, we measured the EOG evoked by the photolysis in mouse OE. An EOG is a transepithelial voltage evoked by activation of multiple receptors in cells at the site of the recording. It is a standard method to assess the net sensitivity of the OE to odorants. Because CyHQ-protected odorants should be delivered to the EOG recording site in solution, we first ensured survival and retention of the odor sensitivity of the tissue after superfusing with a standard phosphate-buffered saline (PBS) solution. An aliquot of PBS (100 μL) was applied on the mouse OE, and then a short 100 ms pulse of amyl acetate (AAc, 1 mM) in the vapor phase was applied after each set of recordings (Figure S11A). The EOG evoked by AAc (1 mM) was used as a reference because it corresponds to the approximate EC₅₀ for activation of EOGs and was used in many studies as a potent olfactory stimulus.⁶⁴ Eugenol as a reference is less suited for this purpose due to its much lower volatility ($P_v = 0.01$ Torr) compared to that of AAc ($P_v = 4.2$ Torr). AAc (1 mM) reproducibly evoked on average 3.51 ± 0.42 mV ($n = 22$, 7 animals). Application of 50–100 μL of either CyHQ-OH or CyHQ-EG (both at 250 μM working concentration in PBS) on the OE surface did not affect or desensitize the OE prior to illumination, as evidenced by a strong EOG response from AAc (1 mM) after the trial (Figure S11B). Illumination of CyHQ-OH treated tissue for up to 5 s with 365 nm light from an LED at 50% power also did not evoke an EOG, confirming

that the photolysis reaction byproduct CyHQ-OH was biologically inert in this assay (Figure S11B).

Illuminating the OE with a 100 ms pulse of 365 nm light from an LED at 50% power after preapplication of 50 μL of CyHQ-EG (250 μM) immediately activated a transient EOG response with a delay of 116.7 ± 6.3 ms and reached a peak amplitude in 344.6 ± 21.9 ms ($n = 16$, 2 animals) (Figure S12), which then returned to its baseline within 5 s, typical of an odor-evoked EOG (Figure 6A).⁶⁴ The delay and rise time of the EOG evoked by a 100 ms pulse of AAc was 104.1 ± 5.9 and 228.7 ± 3.7 ms, respectively ($n = 7$, 3 animals) (Figure S12). Following the first 100 ms pulse, a longer 5 s pulse of 365 nm light evoked a larger response, reaching its peak and then slowly relaxing to a steady-state plateau, again typical of an odor evoked EOG (Figure 6A). These data show that photoreleased eugenol induced an EOG indistinguishable from the vapor-phase odorant evoked response. Importantly, no additionally added CyHQ-EG was required to elicit the second response to a longer 5 s light pulse, suggesting that the pool of CyHQ-EG was not completely depleted during the first light pulse and remained available for subsequent photolysis. Photoreleased eugenol diffused away or was metabolized⁶⁵ fast enough to minimize sensory adaptation and enable multiple stimulations.

Irradiation with a longer wavelength of light (405 nm) at 50% LED power also evoked an EOG using CyHQ-EG (250 μM) (Figure 6B). This outcome was similar to the photoactivation of TRPV1 with 405 nm light (Figure 4). EOG amplitudes were normalized to the EOG evoked by a vapor-phase of AAc (1 mM) presented at the end of each experiment (Figure 6C). A short 100 ms light pulse at 405 nm evoked a significantly smaller EOG than that at 365 nm, 0.144 ± 0.022 ($n = 9$) compared to 0.372 ± 0.064 ($n = 9$, $p = 0.0013$, Mann–Whitney test). The EOG activated with a longer 5 s pulse, however, was not significantly different between 405 and 365 nm, suggesting in both cases that the response was nearly saturated (Figure 6C). Consistent with a larger amplitude of the EOG evoked by 365 nm light, a rise time of the response was also significantly larger than at 405 nm, 344 ± 22 ms ($n = 16$, $p = 0.048$, Mann–Whitney t test) compared to 262 ± 15 ms ($n = 7$) (Figure S12). Surprisingly, delay of the EOG evoked at 365 and 405 nm was not significantly different, 116.7 ± 6.3 ms ($n = 16$) vs 130.4 ± 10.9 ms ($n = 9$, $p = 0.242$, Mann–Whitney t test) (Figure S12).

To better characterize photoactivation, we measured the light intensity dependence of the EOG evoked by light pulses of varying intensity. Following initial treatment with 50 μL of CyHQ-EG (250 μM), 50 ms pulses of 365 nm light from an LED at increasing power output (4–64%) were given at 10 s intervals to allow full recovery (Figure 7A) prior to the next pulse. After adding a fresh 50 μL aliquot of CyHQ-EG (250 μM), the same series of light pulses was given again, but using 405 nm light instead (Figure 7B). Both series of EOGs were recorded at the same spot of the OE. The photoactivated response was normalized to maximal EOG in each series and plotted as a function of relative LED power because we did not measure absolute irradiance at both wavelengths (Figure 7C). Notably, 5-fold more light was required to evoke the same amplitude of the response at 405 nm compared to 365 nm, owing to the fact that photolysis at 365 nm is much more efficient than at 405 nm (Figure 7C) and in line with the absorbance maximum of the CyHQ-protected odorants (see UV–vis spectra in the Supporting Information).

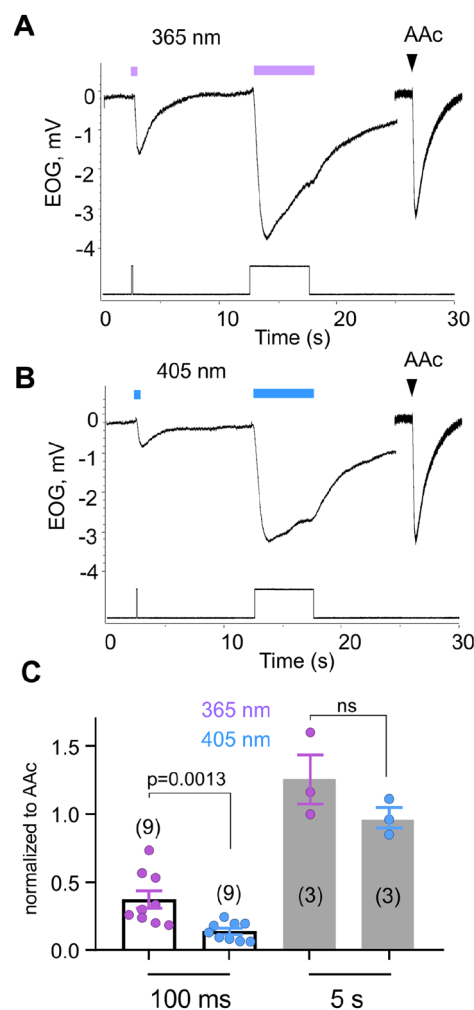


Figure 6. Representative recordings of EOGs measured in mouse olfactory tissue in the presence of 50 μL of CyHQ-EG (250 μM) following exposure to light from an LED at 50% power delivered via a fiber light guide or a 100 ms pressure pulse of AAc (1 mM, black arrowhead) as a positive control. (A) A 100 ms pulse of 365 nm light evoked a transient EOG response, whereas a 5 s light pulse evoked EOG response typical to prolonged odor stimulation. (B) Longer wavelength light (405 nm) also evoked an EOG in the same area of the mouse OE. (C) EOG evoked by 100 ms (empty bars) and 5 s light (gray bars) pulses were normalized to the EOG evoked by AAc (1 mM). The EOG amplitude was significantly larger at 365 nm than at 405 nm, 0.372 ± 0.064 ($n = 9$) compared to 0.144 ± 0.022 ($n = 9$, $p = 0.0013$, Mann–Whitney test). The EOGs evoked by a 5 s pulse of light were not different ($n = 3$, $p = 0.24$, Mann–Whitney test). Adding CyHQ-EG to the tissue prior to illumination did not evoke any significant response or desensitize the tissue, as confirmed by comparing the odor response before and after the addition with AAc. Each data set was collected in different areas of the OE (value of n indicated at each bar) in at least three independent preparations.

The EOG evoked by photolysis of CyHQ-protected benzaldehyde and two thiols was analyzed in a similar manner (Figure 8). Essentially, these photoprotected odorants showed dynamics of the EOG similarly to eugenol. However, CyHQ-BZA was the least potent odorant, activating the smallest response to a 100 ms and 5 s pulse of 365 nm light (Figure 8A, Figure 9). Photoreleased butane-1-thiol was a stronger odorant compared to benzaldehyde and ethanethiol with a latency and rise time to peak of 98.2 ± 5.0 and 250.1 ± 15.9 ms ($n = 17$, 3

animals) for CyHQ-(SBU)₂ vs 126.1 ± 12.2 and 228.7 ± 3.7 ms ($n = 11$, 2 animals) for CyHQ-(SEt)₂, respectively (Figure 9, Figure S12). The small EOG evoked by the photolysis of CyHQ-BZA prevented analysis of the delay and rise time. The difference in the magnitude of the EOG evoked by photolysis of CyHQ-(SBU)₂ and CyHQ-(SEt)₂ was further delineated with a light intensity-response series (Figure S13). Interestingly, the delay between the light pulse and the beginning of the EOG was similar for all the CyHQ-protected odorants, suggesting the availability of odorants in the vicinity of the olfactory receptors, similarly to the case of TRPA1 and TRPV1 channels. The CyHQ-photoprotected odorants can be effectively used to activate a functional response in the mouse OE.

CONCLUSIONS

A set of photoactivatable odorants, CyHQ-EG, -BZ, -2PEA, -(SEt)₂, -(SBU)₂, and -(S-*t*-Bu)₂, was designed and synthesized for use in olfactory tissue preparations. These reagents released the respective odorant upon photolysis at 365 or 405 nm to varying degrees but in sufficient amounts to elicit a physiological response in cell or tissue culture assays. CyHQ-2PEA was the most sensitive to light, whereas CyHQ-(S-*t*-Bu)₂ was the least. Photorelease at 405 nm is important because this wavelength is typically available on most turn-key confocal microscope systems. All of the CyHQ-odorant conjugates activated TRPV1 channels after a brief pulse of light. CyHQ-(SBU)₂ was nearly as effective as the potent capsaicinoid VNA photoreleased from CyHQ-VNA. Only CyHQ-EG and CyHQ-(SBU)₂, however, strongly activated TRPA1 channels. In mouse olfactory epithelial tissue, CyHQ-EG and CyHQ-(SBU)₂ strongly elicited a dose-dependent EOG response rapidly after brief light exposure that will enable precise control of OSN activation for the study of the kinetics and pharmacology of olfaction. These tools will be valuable for the study of chemosensory systems in model organisms.

METHODS

Synthesis. General. All reagents and solvents were purchased from commercial sources and used without further purification. ¹H NMR and ¹³C NMR were recorded on a Bruker Avance III HD 500 or 600 MHz NMR spectrometer. HPLC and uHPLC (analytical and preparative) were performed on an Agilent Infinity series system with an autosampler and diode array detector using Zorbax eclipse C-18 reverse phase columns. HRMS was performed on an Agilent 6540 HD Accurate Mass QTOF/LC/MS with electrospray ionization (ESI) or a Micromass QTOF-Ultima with ESI. KMOPS buffer consisted of 100 mM KCl and 10 mM MOPS titrated to pH 7.2 with KOH. Flash chromatography was performed on an Isolera Spektra 4 with Biotage SNAP cartridges packed with KPSIL silica.

7-(Methoxymethoxy)-2-vinylquinoline-8-carbonitrile (3). Methyltriphenylphosphonium bromide (1.32 g, 3.7 mmol, 1.2 equiv) and potassium carbonate (0.685 g, 5 mmol, 1.6 equiv) was added to dry THF (15 mL) and stirred at RT for 15 min. Aldehyde 2 (0.750 g, 3.1 mmol, 1 equiv), was dissolved in dry THF and added dropwise to the mixture over 10 min. The mixture was heated to reflux for 6 h. The mixture was cooled then concentrated in vacuo, and the resulting residue was subjected to flash column chromatography (25% EtOAc in hexane) to yield alkene 3 as a pale yellow solid (0.469 g, 63%): ¹H NMR (500 MHz, methanol-*d*₄, δ): 8.31 (d, $J = 8.5$ Hz, 1H), 8.15 (d, $J = 9.2$ Hz, 1H), 7.72 (d, $J = 8.5$ Hz, 1H), 7.64 (d, $J = 9.1$ Hz, 1H), 7.08 (dd, $J = 17.6, 10.8$ Hz, 1H), 6.54 (dd, $J = 17.6, 1.1$ Hz, 1H), 5.76 (dd, $J = 10.8, 1.1$ Hz, 1H), 5.54 (s, 2H), 3.60 (s, 3H); ¹³C NMR (126 MHz, methanol-*d*₄, δ): 162.5, 158.3, 148.4, 137.0, 136.8, 133.8, 122.8,

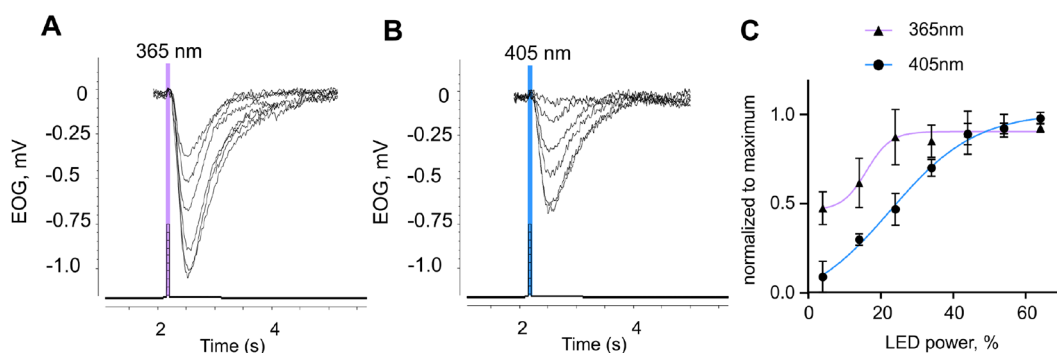


Figure 7. Irradiation dependence of the mouse EOG evoked by photolysis of CyHQ-EG at (A) 365 and (B) 405 nm. Representative data collected from the same preparation. An aliquot (50 μL) of CyHQ-EG (250 μM) was applied once to the OE before running a series of pulses at either wavelength. A short 100 ms pulse of both wavelengths irradiated the same area of the tissue, increasing LED power from 4 to 64% of the maximum. A recovery period of 20 s was allowed between each consecutive light pulse. (C) Dependence of the EOG evoked as a function of irradiation LED power. Individual EOG amplitudes were normalized to the maximum value in each series. Each data point was calculated from at least three replicates in two animals and different areas of the OE. Data are presented as the mean \pm SEM.

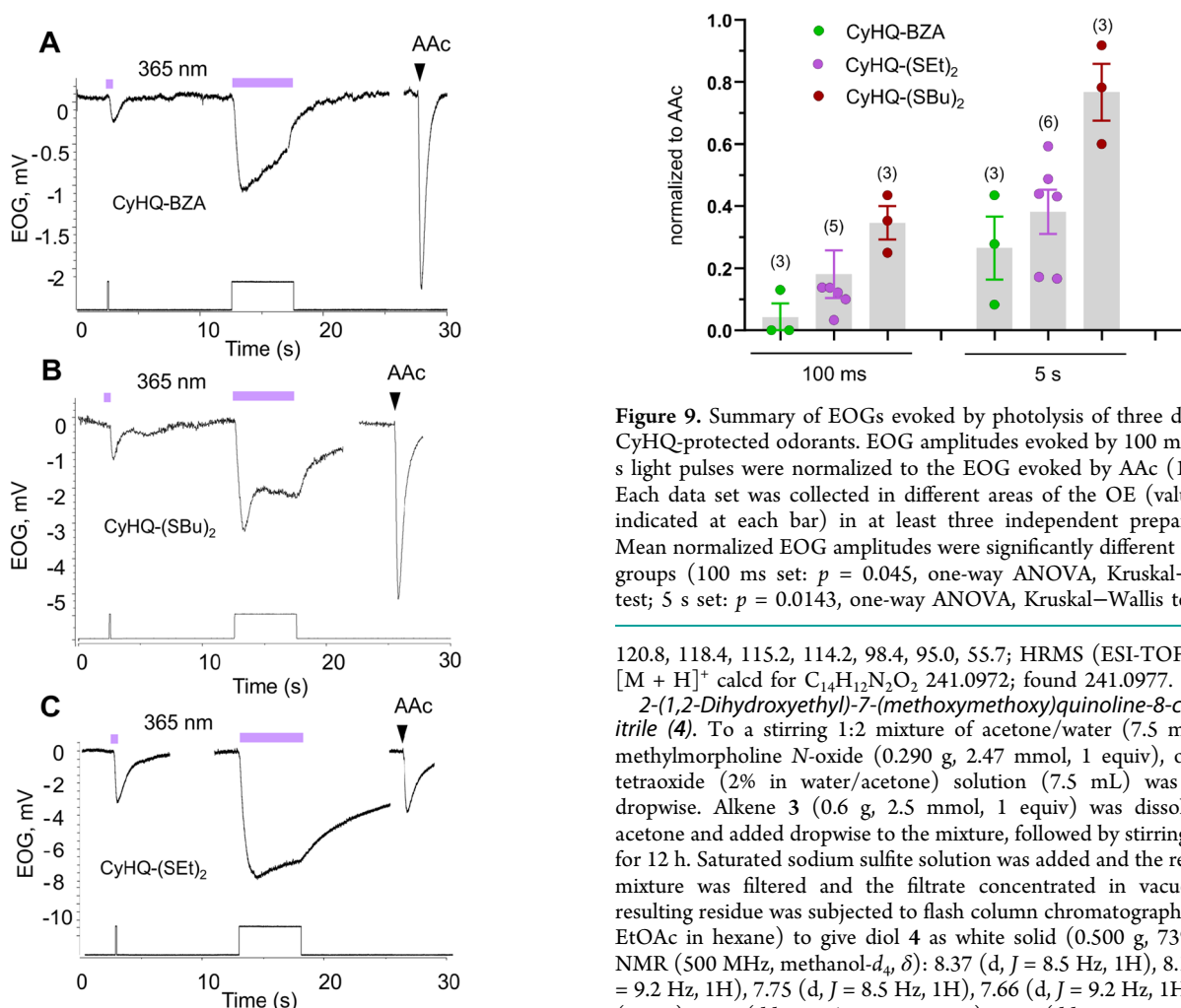


Figure 8. EOGs measured in mouse olfactory tissue following photolysis of other CyHQ-protected odorants by 365 nm LED light at 50% power delivered via a fiber light guide or application of vaporized solution of AAc (1 mM, black arrowhead) as a positive control. A 100 ms pulse of 365 nm light evoked a transient EOG response, whereas a 5 s light pulse evoked a typical EOG response. CyHQ-protected odorants were (A) benzaldehyde, (B) ethanethiol, and (C) butane-1-thiol.

Figure 9. Summary of EOGs evoked by photolysis of three different CyHQ-protected odorants. EOG amplitudes evoked by 100 ms and 5 s light pulses were normalized to the EOG evoked by AAc (1 mM). Each data set was collected in different areas of the OE (value of n indicated at each bar) in at least three independent preparations. Mean normalized EOG amplitudes were significantly different in both groups (100 ms set: $p = 0.045$, one-way ANOVA, Kruskal–Wallis test; 5 s set: $p = 0.0143$, one-way ANOVA, Kruskal–Wallis test).

120.8, 118.4, 115.2, 114.2, 98.4, 95.0, 55.7; HRMS (ESI-TOF) m/z : $[\text{M} + \text{H}]^+$ calcd for $\text{C}_{14}\text{H}_{12}\text{N}_2\text{O}_2$ 241.0972; found 241.0977.

2-(1,2-Dihydroxyethyl)-7-(methoxymethoxy)quinoline-8-carbonitrile (4). To a stirring 1:2 mixture of acetone/water (7.5 mL), *N*-methylmorpholine *N*-oxide (0.290 g, 2.47 mmol, 1 equiv), osmium tetroxide (2% in water/acetone) solution (7.5 mL) was added dropwise. Alkene 3 (0.6 g, 2.5 mmol, 1 equiv) was dissolved in acetone and added dropwise to the mixture, followed by stirring at RT for 12 h. Saturated sodium sulfite solution was added and the resulting mixture was filtered and the filtrate concentrated in vacuo. The resulting residue was subjected to flash column chromatography (90% EtOAc in hexane) to give diol 4 as white solid (0.500 g, 73%): ^1H NMR (500 MHz, methanol- d_4 , δ): 8.37 (d, $J = 8.5$ Hz, 1H), 8.18 (d, $J = 9.2$ Hz, 1H), 7.75 (d, $J = 8.5$ Hz, 1H), 7.66 (d, $J = 9.2$ Hz, 1H), 5.54 (s, 2H), 4.98 (dd, $J = 6.1, 4.4$ Hz, 1H), 4.03 (dd, $J = 11.4, 4.4$ Hz, 1H), 3.89 (dd, $J = 11.4, 6.1$ Hz, 1H), 3.59 (s, 3H); ^{13}C NMR (126 MHz, methanol- d_4 , δ): 164.8, 162.4, 147.5, 137.0, 134.1, 122.8, 118.6, 115.4, 114.2, 98.2, 95.0, 74.7, 66.1, 55.8; HRMS (ESI-TOF) m/z : $[\text{M} + \text{H}]^+$ calcd for $\text{C}_{14}\text{H}_{14}\text{N}_2\text{O}_4$ 275.1026; found 275.1032.

7-Hydroxy-2-(2-phenyl-1,3-dioxolan-4-yl)quinoline-8-carbonitrile (CyHQ-BZA). Diol 4 (0.050 g, 0.18 mmol, 1 equiv), anhydrous iron(III) chloride (0.059 mg, 0.36 mmol, 2 equiv), and (dimethoxymethyl)benzene (0.132 mL, 0.91 mmol, 5 equiv) was refluxed in dry THF for 24 h or when LCMS indicated the reaction was complete. The mixture was cooled, then concentrated in vacuo.

The resulting residue was subjected to flash column chromatography (10:90 hexane/EtOAc) to yield a 2:1 mixture of CyHQ-BZA diastereomers (0.020 g, 35%): Diastereomer 1: ^1H NMR (500 MHz, methanol- d_4 , δ): 8.22 (dd, $J = 8.4, 5.5$ Hz, 1H), 7.98 (dq, $J = 9.1, 4.5$ Hz, 1H), 7.64–7.55 (m, 3H), 7.47–7.39 (m, 3H), 7.24 (dt, $J = 9.1, 2.9$ Hz, 1H), 6.05 (d, $J = 2.1$ Hz, 1H), 5.49 (tdd, $J = 7.6, 5.8, 2.5$ Hz, 1H), 4.56 (td, $J = 8.0, 2.3$ Hz, 1H), 4.38 (ddd, $J = 8.3, 5.0, 1.3$ Hz, 1H); ^{13}C NMR (126 MHz, methanol- d_4 , δ): 162.8, 148.4, 137.2, 133.8, 129.1, 128.0, 126.6, 121.6, 118.0, 116.8, 114.9, 105.1, 94.3, 78.8, 71.0, 54.6, 28.1; Diastereomer 2: ^1H NMR (500 MHz, methanol- d_4 , δ): 8.28 (dd, $J = 8.4, 5.5$ Hz, 1H), 8.05–7.99 (m, 1H), 7.67 (dd, $J = 8.3, 3.9$ Hz, 1H), 7.64–7.55 (m, 2H), 7.49–7.38 (m, 3H), 6.21 (d, $J = 2.0$ Hz, 1H), 5.49 (tdd, $J = 7.6, 5.8, 2.5$ Hz, 2H), 4.70 (ddd, $J = 8.9, 6.9, 2.1$ Hz, 1H), 4.26 (ddd, $J = 8.3, 6.5, 1.8$ Hz, 1H); ^{13}C NMR (126 MHz, methanol- d_4 , δ): 164.7, 148.7, 137.4, 133.8, 129.1, 128.0, 126.4, 121.6, 118.0, 116.7, 114.9, 104.8, 94.3, 78.4, 70.7, 54.6, 30.7; HRMS (ESI-TOF) m/z : $[\text{M} + \text{H}]^+$ calcd for $\text{C}_{19}\text{H}_{14}\text{N}_2\text{O}_3$ 319.1077; found 319.1083.

(8-Cyano-7-hydroxyquinolin-2-yl)methyl phenethylcarbamate (CyHQ-2PEA). 2-Phenethylamine (0.1 g, 0.83 mmol, 1 equiv), triethylamine (0.690 mL, 4.95 mmol, 6 equiv), and 1,1'-carbonyldiimidazole (0.401 g, 2.47 mmol, 3 equiv) were stirred together at RT. Water was added and the mixture was filtered, dried over anhydrous sodium sulfate, and concentrated. The resulting residue was dissolved in dichloromethane (4 mL) followed by addition of triethylamine (0.432 mL, 3.1 mmol, 5 equiv), MOM-CyHQ-OH (0.151 g, 0.62 mmol, 1 equiv). Once TLC indicated the reaction to be complete, water was added and the resulting mixture was concentrated in vacuo. The resulting residue was treated with a 1:1 solution of TFA/ CH_2Cl_2 (5 mL) for 12 h and then concentrated in vacuo. The resulting residue was subjected to flash column chromatography (95:5 $\text{CH}_2\text{Cl}_2/\text{MeOH}$) to provide CyHQ-2PEA (0.133 g, 62%): ^1H NMR (500 MHz, methanol- d_4 , δ): 8.23 (d, $J = 8.4$ Hz, 1H), 7.99 (d, $J = 9.0$ Hz, 1H), 7.37 (d, $J = 8.4$ Hz, 1H), 7.32–7.16 (m, 7H), 5.34 (s, 2H), 3.40 (t, $J = 7.4$ Hz, 2H), 2.84 (t, $J = 7.4$ Hz, 2H); ^{13}C NMR (126 MHz, methanol- d_4 , δ): 164.2, 160.0, 157.1, 148.3, 139.1, 137.2, 133.8, 128.5, 128.1, 125.9, 121.5, 117.6, 117.0, 114.7, 94.2, 66.5, 42.1, 35.7; HRMS (ESI-TOF) m/z : $[\text{M} + \text{H}]^+$ calcd for $\text{C}_{20}\text{H}_{17}\text{N}_3\text{O}_3$ 348.1343; found 348.1348.

2-((4-Allyl-2-methoxyphenoxy)methyl)-7-hydroxyquinoline-8-carbonitrile (CyHQ-EG). To a microwave reaction vial, MOM-CyHQ-OMs (0.065 g, 0.20 mmol, 1 equiv), eugenol (0.041 mL, 0.26 mmol, 1.3 equiv), and potassium carbonate (0.083 g, 0.60 mmol, 3 equiv) were added to dimethylformamide (1 mL). The resulting mixture was stirred with microwave heating at 90 °C for 30 min, then cooled and concentrated in vacuo. The resulting residue was subjected to flash column chromatography (90:10 $\text{CH}_2\text{Cl}_2/\text{MeOH}$) to provide CyHQ-EG as yellow semisolid (0.040 g, 57% yield): ^1H NMR (500 MHz, methanol- d_4 , δ): 8.25 (d, $J = 8.4$ Hz, 1H), 7.99 (d, $J = 9.1$ Hz, 1H), 7.67 (d, $J = 8.4$ Hz, 1H), 7.25 (d, $J = 9.1$ Hz, 1H), 6.97 (d, $J = 8.2$ Hz, 1H), 6.76–6.65 (m, 1H), 5.96 (ddt, $J = 16.8, 10.0, 6.7$ Hz, 1H), 5.36 (s, 2H), 5.13–4.96 (m, 2H), 3.89 (s, 3H), 3.86–3.69 (m, 2H), 1.45–1.17 (m, 2H); ^{13}C NMR (126 MHz, methanol- d_4 , δ): 164.7, 160.7, 149.6, 148.5, 146.2, 137.7, 137.1, 134.0, 133.8, 121.5, 120.4, 118.0, 117.5, 115.0, 114.4, 114.3, 112.7, 94.1, 71.8, 55.1, 39.3; HRMS (ESI-TOF) m/z : $[\text{M} + \text{H}]^+$ calcd for $\text{C}_{21}\text{H}_{18}\text{N}_2\text{O}_3$ 347.1390; found 347.1396.

General Procedure for the Preparation of CyHQ-Protected Thiols. Aldehyde 2 (0.83 mmol, 1 equiv), 12 M hydrochloric acid (4 mL), and alkanethiol (4.15 mmol, 5 equiv) were combined and stirred at RT. When LCMS analysis indicated that the reaction was complete, a saturated solution of sodium bicarbonate was added followed by ethyl acetate. The ethyl acetate layer was concentrated in vacuo, and the resulting residue subjected to flash column chromatography using hexane/EtOAc as the eluent to provide the corresponding CyHQ-protected thiol.

2-(Bis(ethylthio)methyl)-7-hydroxyquinoline-8-carbonitrile (CyHQ-(SEt))₂. 69% yield. ^1H NMR (500 MHz, chloroform- d , δ): 8.08 (d, $J = 8.5$ Hz, 1H), 7.82 (d, $J = 9.0$ Hz, 1H), 7.65 (d, $J = 8.4$ Hz, 1H), 7.33 (d, $J = 9.0$ Hz, 1H), 6.79 (s, 1H), 5.25 (s, 1H), 2.75–2.60 (m,

4H), 1.26 (t, $J = 7.4$ Hz, 6H); ^{13}C NMR (126 MHz, chloroform- d , δ): 163.9, 162.7, 147.5, 137.6, 133.7, 121.7, 119.0, 118.8, 115.5, 94.9, 54.1, 26.4, 14.4; HRMS (ESI-TOF) m/z : $[\text{M} + \text{H}]^+$ calcd for $\text{C}_{15}\text{H}_{16}\text{N}_2\text{O}_2\text{S}_2$ 305.0777; found 305.0803.

2-(Bis(butylthio)methyl)-7-hydroxyquinoline-8-carbonitrile (CyHQ-(SBU))₂. 75% yield. ^1H NMR (500 MHz, chloroform- d , δ): 7.93 (d, $J = 8.4$ Hz, 1H), 7.66 (d, $J = 8.9$ Hz, 1H), 7.56 (d, $J = 8.4$ Hz, 1H), 7.23 (d, $J = 9.0$ Hz, 1H), 6.21 (s, 1H), 5.16 (s, 1H), 2.66 (t, $J = 7.6$ Hz, 4H), 1.57 (tt, $J = 8.4, 6.2$ Hz, 4H), 1.41–1.32 (m, 4H), 0.86 (t, $J = 7.4$ Hz, 6H); ^{13}C NMR (126 MHz, chloroform- d , δ): 164.3, 162.5, 147.7, 137.2, 133.5, 121.2, 119.4, 118.3, 116.5, 94.8, 54.9, 32.0, 31.3, 22.0, 13.6; HRMS (ESI-TOF) m/z : $[\text{M} + \text{H}]^+$ calcd for $\text{C}_{19}\text{H}_{24}\text{N}_2\text{O}_2\text{S}_2$ 361.1403; found 361.1433.

2-(Bis(tert-butylthio)methyl)-7-hydroxyquinoline-8-carbonitrile (CyHQ-(S-t-Bu))₂. 85% yield. ^1H NMR (500 MHz, chloroform- d , δ): 8.08 (d, $J = 8.5$ Hz, 1H), 7.87 (d, $J = 9.0$ Hz, 1H), 7.77 (d, $J = 8.5$ Hz, 1H), 7.25 (d, $J = 8.9$ Hz, 1H), 5.39 (s, 1H), 1.32 (s, 18H); ^{13}C NMR (126 MHz, chloroform- d , δ): 166.8, 162.2, 147.0, 136.8, 133.7, 121.8, 120.5, 118.0, 115.0, 95.6, 49.8, 46.7, 31.1; HRMS (ESI-TOF) m/z : $[\text{M} + \text{H}]^+$ calcd for $\text{C}_{19}\text{H}_{24}\text{N}_2\text{O}_2\text{S}_2$ 361.1403; found 361.1408.

Photolysis Reactions. Solutions of the CyHQ-protected odorants (0.1 mM) were prepared in KMOPS buffer. Solutions were placed in a 3 mL quartz cuvette and continuously stirred with a stirring bar. Irradiation was carried out with an LED lamp (Cairn OptoLED Lite) at 365 and 405 nm with constant stirring. The lamp intensity was measured by ferrioxalate actinometry.⁶⁶ Aliquots (50 μL) were sampled at different time intervals and analyzed by reverse-phase uHPLC. Three repeats were carried out for each experiment. HPLC analysis was performed on an Agilent 1290 Infinity series uHPLC using a Zorbax Eclipse Plus C18 column, monitoring the AUC at 320 nm. Separations were carried out with a gradient elution (flux rate of 0.3 mL/min) using a mobile phase composed of A = 0.1% trifluoroacetic acid in water and B = acetonitrile (starting from 5% B to 100% over 12 min and re-equilibrating to 5% B before the next run). The quantification of the percentage of the starting material remaining was performed by comparison of the AUC measured with calibration curves created from known concentrations of the substrate (external standard method). Percent remaining was plotted versus time. The time in seconds for 90% of starting material to be consumed ($t_{90\%}$) was obtained by fitting a single exponential decay curve to the data using DeltaGraph (Red Rock Software). The quantum efficiency (Φ_u) of the photolysis reaction was calculated from the following equation:

$$\Phi_u = (I\sigma t_{90\%})^{-1}$$

where $t_{90\%}$ = time required to consume 90% of the starting material, I represents the lamp intensity in Einstein $\text{cm}^{-2} \text{s}^{-1}$, and σ is the decadic extinction coefficient ($1000 \times \epsilon$, molar extinction coefficient) (Table S1).^{24,26,67} The release of benzaldehyde, phenethylamine, and eugenol was quantified by monitoring the AUC at 280 nm and plotted vs time, fitting an exponential rise to max curve to the data.

Determination of the Stability toward Spontaneous Hydrolysis in the Dark. Solutions of each CyHQ-protected odorant (0.1 mM) in KMOPS buffer were kept in the dark and sampled at different time intervals over 7 days. The percentage of starting material remaining was determined by HPLC analysis as described for the photolysis reactions.

Cell Culture. Heterologous Expression and Transient Transfection of TRPV1 and TRPA1 in HEK 293 Cells. HEK 293T cells were grown in HEK media [DMEM, 10% FBS (MP Biomedicals), L-glutamine (2 mM), and penicillin/streptomycin (100 $\mu\text{g}/\text{mL}$) (Invitrogen)] at 37 °C with 5% CO_2 . The hTRPA1 channel was transiently expressed in the cells from the recombinant expression plasmid pcDNA5-FRT carrying the entire protein coding region for hTRPA1 (gift of Dr. Gisselman, Bochum University, Germany). The hTRPV1 channel was transiently expressed using the plasmid pCMV6-NEO-TRPV1 plasmid (Origene). Semiconfluent HEK 293T cells in 35 mm dishes were transiently cotransfected with 1 μg of pcDNA5-FRT/hTRPA1 and 0.2 μg of a separate plasmid (pXoon) carrying the coding sequence for green fluorescent protein

(GFP) using Calcectin reagent (SigmaGen). At 24–48 h post-transfection, the cells were gently lifted from the dishes using 2 mM EDTA in phosphate-buffered saline, washed with HEK media, replated as individual cells/small clusters in HEK media without antibiotics on 35 mm plates, and allowed to recover for at least 2 h prior to electrophysiology.

Stably Transfected HEK 293 Cells Expressing TRPV1. HEK 293 cells were cultured in DMEM media with 10% FBS and 1% penicillin/streptomycin in cell culture flasks at 37 °C and 5% CO₂. HEK 293 cells stably expressing TRPV1 were created by transfection with a pCMV6-NEO-TRPV1 plasmid (Origene) using TrueFect reagent (United BioSystems) and G418 (600 µg/mL) for selection. The cells were cultured in DMEM media with 10% FBS and 1% PEN-STREP. G418 antibiotic (300 µg/mL) was used for maintaining the stable expression of TRPV1.

Whole-Cell Patch Clamp Recording. Human TRPA1 and TRPV1 ion currents were investigated using whole-cell patch clamp recording. The current was measured with a 200B patch clamp amplifier (Molecular Devices) and a digital interface (Digidata 1320A, Molecular Devices), lowpass filtered at 5–10 kHz, sampled at 2–20 kHz, and in most cases digitally filtered at 1–1.4 kHz. Analysis of the data was carried out using pCLAMP 9.2 software (Molecular Devices). Membrane voltage was held at –60 mV. Patch pipettes were fabricated from borosilicate capillary glass (BF150–86–10, Sutter Instrument) using a Flaming–Brown micropipette puller (P-87, Sutter Instrument). The fire polished patch pipet had a resistance of about 5 MΩ when filled with a solution composed of KCl (140 mM), EGTA (1 mM), and Hepes (10 mM) adjusted to pH 7.4 with KOH. To measure TRPA1 current, the pipet solution was supplemented with sodium pyrophosphate (1 mM), which is known to protect the channels from the run-down.⁶⁸ Normal Ringer solution was used as a bath solution and contained NaCl (140 mM), MgCl₂ (1 mM), CaCl₂ (1 mM), and HEPES (10 mM) adjusted to pH 7.4 with NaOH. To measure maximal TRPA1 currents no Ca²⁺ was added to the bath solution whereby preventing calcium-dependent desensitization of the channels.⁶⁹ Bath exchange was performed using a rapid solution changer with a modified tube holder, RSC-160 (Bio-Logic, Claix, France). Data were recorded under continuous superfusion with Ringer solution alone or supplemented with indicated concentration of CyHQ reagents for 30 s. This time period started 10 s before applying the LED light pulse. GFP-positive HEK 293T cells were visualized using an Axiovert 100 inverted microscope (Carl Zeiss) equipped with a mercury arc lamp (HBO100) coupled to the GFP filter set (Ex BP 475/40, Em 530/50, 1114–459, Zeiss). The sample illumination time did not exceed 20 s to minimize any possible phototoxicity and aberrant activation of TRPA1 channels.⁷⁰ The LED light source (Prizmatix) generating 365 and 405 nm light was triggered by Clampfit 9.2 software in-line with the whole-cell current recording.

Live Cell Imaging of Calcium and TRPV1 Activation. Live cell imaging was carried out on an Olympus FluoView FV1000MPE confocal microscope. Excitation using an argon ion laser was set at 488 nm, and emitted light was reflected through a 500–600 nm filter from a dichroic mirror. Data capture and extraction was carried out with FluoView 10-ASW version 4.0 (Olympus), ImageJ-Fiji, and DeltaGraph (Red Rock Software).

Calcium Dye Loading. One day prior to the experiment, HEK 293 cells (stably expressing TRPV1 channels) were plated on 35 mm glass bottom dish (previously coated with poly-D-Lysine). Fluo-4 AM (50 µg, Life Technologies) was dissolved in DMSO (50 µL) and added with Pluronic F-127 (Molecular Probes) to HBSS and sonicated for 5 min to create a solution containing a 0.02% final concentration of each. The solution was loaded onto the cells growing in the 35 mm glass bottom dish and incubated for 30 min in a humidified CO₂ incubator (37 °C, 5% CO₂). The cells were washed with HBSS and maintained in HBSS during the photoactivation experiments.

TRPV1 Activation on HEK 293 Cells. The 405 nm laser integrated on the confocal microscope was used for excitation. Solutions of CyHQ-protected odorants or VNA were added to the culture dish

from a pipet and a defined area near a cell was irradiated with a short (10–200 ms) pulse of 405 nm laser light while imaging at 488 nm.

Mouse Electroolfactograms (EOGs). Adult C57/B6 mice of both sexes were used in this study approved by the University of Florida IACUC protocol 201608162. Mice were anesthetized with CO₂, rapidly decapitated, and the head split along the cranial midline. Septal tissue was removed to expose olfactory turbinates. AAC in the vapor-phase was delivered as a short 100 ms pulse by a pressurized nitrogen line connected to a sealed 100 mL glass bottle and directly injected into a continuous stream of humidified carbogen flowing over the tissue. AAC was prepared by diluting a 1 M stock solution into deionized water to generate a final working concentration. EOGs were recorded with a standard glass micropipette tip-filled with agarose and backfilled with a standard phosphate-buffered saline (PBS) using a Multiclamp 700A amplifier controlled by Multiclamp 700A and Clampex 9.2 software (Molecular Devices). EOGs were measured as the maximal peak amplitude from the prepulse baseline using Clampfit 9.2 software (Molecular devices). An LED light source (Prizmatix) generating 365 and 405 nm light was triggered by Clampfit 9.2 software in-line with the whole-cell current recording. Delay of the EOG and rise time from baseline to the peak was measured using Clampfit 9.2 software.

Reagents for Patch Clamp Recording and Electroolfactograms. CyHQ reagents were prepared as a 200 mM stock in DMSO and kept at –20 °C until needed. Freshly made working solutions, typically 250 µM, were made from the stock by adding directly to PBS and sonicating. Eugenol and AAC were prepared as a 1 M stock in DMSO. Eugenol was applied as a working solution in PBS at the concentration indicated for each experiment. AAC was prepared as a solution in ultrapure water at nominal concentration of 1 mM and applied to the mouse nasal preparation as a vapor phase. All experiments were performed under dimmed room light which did not induce any measurable activation of either TRP channels or mouse EOG.

■ ASSOCIATED CONTENT

Supporting Information

The Supporting Information is available free of charge at <https://pubs.acs.org/doi/10.1021/acscchembio.0c00541>.

Figures S1–S13, Table S1, ¹H and ¹³C NMR spectra, and UV–vis spectra (PDF)

■ AUTHOR INFORMATION

Corresponding Authors

Timothy M. Dore – New York University Abu Dhabi, Abu Dhabi, United Arab Emirates; Department of Chemistry, University of Georgia, Athens, Georgia 30602, United States; orcid.org/0000-0002-3876-5012; Email: timothy.dore@nyu.edu

Jeffrey R. Martens – Department of Pharmacology and Therapeutics and Center for Smell and Taste, University of Florida, Gainesville, Florida 32610, United States; Email: martensj@ufl.edu

Authors

Sangram Gore – New York University Abu Dhabi, Abu Dhabi, United Arab Emirates; orcid.org/0000-0003-4236-7604

Kirill Ukhanov – Department of Pharmacology and Therapeutics and Center for Smell and Taste, University of Florida, Gainesville, Florida 32610, United States; orcid.org/0000-0003-0633-9067

Cyril Herbivo – New York University Abu Dhabi, Abu Dhabi, United Arab Emirates

Naeem Asad – New York University Abu Dhabi, Abu Dhabi, United Arab Emirates; orcid.org/0000-0001-6871-5270

Yuriy V. Bobkov – Department of Pharmacology and Therapeutics and Whitney Laboratory for Marine Bioscience, University of Florida, Gainesville, Florida 32610, United States

Complete contact information is available at:
<https://pubs.acs.org/10.1021/acscchembio.0c00541>

Author Contributions

[†]S.G. and K.U. contributed equally.

Funding

This research was supported by New York University Abu Dhabi (T.M.D.) and by US Public Health Service Grant NIH/NIDCD R01DC009606 (J.R.M.).

Notes

The authors declare no competing financial interest.

ACKNOWLEDGMENTS

Part of this work was carried out using Core Technology Platform resources at New York University Abu Dhabi.

REFERENCES

- (1) Axel, R. (1995) The molecular logic of smell. *Sci. Am.* 273, 154–159.
- (2) Jones, N., and Rog, D. (1998) Olfaction: A Review. *J. Laryngol. Otol.* 112, 11–24.
- (3) Bhandawat, V., Reiser, J., and Yau, K.-W. (2005) Elementary Response of Olfactory Receptor Neurons to Odorants. *Science* 308, 1931–1934.
- (4) DeMaria, S., and Ngai, J. (2010) The cell biology of smell. *J. Cell Biol.* 191, 443–452.
- (5) Li, W. (2014) Learning to smell danger: acquired associative representation of threat in the olfactory cortex. *Front. Behav. Neurosci.* 8, 98.
- (6) Sullivan, R. M., Wilson, D. A., Ravel, N., and Mouly, A.-M. (2015) Olfactory memory networks: from emotional learning to social behaviors. *Front. Behav. Neurosci.* 9, 36.
- (7) Yang, S.-Y., Walther, B. A., and Weng, G.-J. (2015) Stop and smell the pollen: the role of olfaction and vision of the oriental honey buzzard in identifying food. *PLoS One* 10, No. e0130191.
- (8) Teodoro-Morrison, T., Diamandis, E. P., Rifai, N., Weetjens, B. J. C., Pennazza, G., de Boer, N. K., and Bomers, M. K. (2014) Animal olfactory detection of disease: promises and pitfalls. *Clin. Chem.* 60, 1473–1479.
- (9) Ferdenzi, C., Licon, C., and Bensafi, M. (2017) Detection of sickness in conspecifics using olfactory and visual cues. *Proc. Natl. Acad. Sci. U. S. A.* 114, 6157–6159.
- (10) Jacobs, L. F., Arter, J., Cook, A., and Sulloway, F. J. (2015) Olfactory orientation and navigation in humans. *PLoS One* 10, No. e0129387.
- (11) Dahmani, L., Patel, R. M., Yang, Y., Chakravarty, M. M., Fellows, L. K., and Bohbot, V. D. (2018) An intrinsic association between olfactory identification and spatial memory in humans. *Nat. Commun.* 9, 4162.
- (12) Baum, M. J. (2012) Contribution of pheromones processed by the main olfactory system to mate recognition in female mammals. *Front. Neuroanat.* 6, 20.
- (13) Oboti, L., Schellino, R., Giachino, C., Chamero, P., Pyrski, M., Leinders-Zufall, T., Zufall, F., Fasolo, A., and Peretto, P. (2011) Newborn interneurons in the accessory olfactory bulb promote mate recognition in female mice. *Front. Neurosci.* 5, 113.
- (14) Yeomans, M. R. (2006) Olfactory influences on appetite and satiety in humans. *Physiol. Behav.* 87, 800–804.
- (15) Negroni, J., Meunier, N., Monnerie, R., Salesse, R., Baly, C., Caillol, M., and Congar, P. (2012) Neuropeptide Y enhances olfactory mucosa responses to odorant in hungry rats. *PLoS One* 7, No. e45266.
- (16) Connor, E. E., Zhou, Y., and Liu, G. E. (2018) The essence of appetite: does olfactory receptor variation play a role? *J. Anim. Sci.* 96, 1551–1558.
- (17) Malnic, B., Hirono, J., Sato, T., and Buck, L. B. (1999) Combinatorial receptor codes for odors. *Cell* 96, 713–723.
- (18) Zou, D.-J., Chesler, A., and Firestein, S. (2009) How the olfactory bulb got its glomeruli: A just so story? *Nat. Rev. Neurosci.* 10, 611–618.
- (19) Young, J. M., Shykind, B. M., Lane, R. P., Tonnes-Priddy, L., Ross, J. A., Walker, M., Williams, E. M., and Trask, B. J. (2003) Odorant receptor expressed sequence tags demonstrate olfactory expression of over 400 genes, extensive alternate splicing and unequal expression levels. *Genome Biol.* 4, R71.
- (20) Mombaerts, P. (2004) Genes and ligands for odorant, vomeronasal and taste receptors. *Nat. Rev. Neurosci.* 5, 263–278.
- (21) Laska, M., Ayabe-Kanamura, S., Hubener, F., and Saito, S. (2000) Olfactory discrimination ability for aliphatic odorants as a function of oxygen moiety. *Chem. Senses* 25, 189–197.
- (22) Firestein, S. (2001) How the olfactory system makes sense of scents. *Nature* 413, 211–218.
- (23) Buck, L., and Axel, R. (1991) A novel multigene family may encode odorant receptors: a molecular basis for odor recognition. *Cell* 65, 175–187.
- (24) Davis, M. J., Kragor, C. H., Reddie, K. G., Wilson, H. C., Zhu, Y., and Dore, T. M. (2009) Substituent Effects on the Sensitivity of a Quinoline Photoremovable Protecting Group to One- and Two-Photon Excitation. *J. Org. Chem.* 74, 1721–1729.
- (25) McLain, D. E., Rea, A. C., Widegren, M. B., and Dore, T. M. (2015) Photoactivatable, biologically-relevant phenols with sensitivity toward 2-photon excitation. *Photochem. Photobiol. Sci.* 14, 2151–2158.
- (26) Asad, N., Deodato, D., Lan, X., Widegren, M. B., Phillips, D. L., Du, L., and Dore, T. M. (2017) Photochemical Activation of Tertiary Amines for Applications in Studying Cell Physiology. *J. Am. Chem. Soc.* 139, 12591–12600.
- (27) O'Connor, M. J., Beebe, L. L., Deodato, D., Ball, R. E., Page, A. T., VanLeuven, A. J., Harris, K. T., Park, S., Hariharan, V., Lauderdale, J. D., and Dore, T. M. (2019) Bypassing Glutamic Acid Decarboxylase 1 (Gad1) Induced Craniofacial Defects with a Photoactivatable Translation Blocker Morpholino. *ACS Chem. Neurosci.* 10, 266–278.
- (28) Walpole, C. S. J., and Wrigglesworth, R. (1993) Structural requirements for capsaicin agonists and antagonists. In *Capsaicin in the Study of Pain* (Wood, J. N., Ed.), pp 63–81, Academic Press, London.
- (29) Caterina, M. J., Schumacher, M. A., Tominaga, M., Rosen, T. A., Levine, J. D., and Julius, D. (1997) The capsaicin receptor: a heat-activated ion channel in the pain pathway. *Nature* 389, 816–824.
- (30) Clapham, D. E., Runnels, L. W., and Strubing, C. (2001) The TRP ion channel family. *Nat. Rev. Neurosci.* 2, 387–396.
- (31) Clapham, D. E. (2003) TRP channels as cellular sensors. *Nature* 426, 517–524.
- (32) Karai, L. J., Russell, J. T., Iadarola, M. J., and Olah, Z. (2004) Vanilloid Receptor 1 regulates multiple calcium compartments and contributes to Ca²⁺-induced Ca²⁺ release in sensory neurons. *J. Biol. Chem.* 279, 16377–16387.
- (33) Gilbert, D., Funk, K., Dekowski, B., Lechler, R., Keller, S., Moehrlen, F., Frings, S., and Hagen, V. (2007) Caged capsaicins: new tools for the examination of TRPV1 channels in somatosensory neurons. *ChemBioChem* 8, 89–97.
- (34) Zemelman, B. V., Nesnas, N., Lee, G. A., and Miesenböck, G. (2003) Photochemical gating of heterologous ion channels: Remote control over genetically designated populations of neurons. *Proc. Natl. Acad. Sci. U. S. A.* 100, 1352–1357.
- (35) Zhao, J., Gover, T. D., Muralidharan, S., Auston, D. A., Weinreich, D., and Kao, J. P. Y. (2006) Caged Vanilloid Ligands for Activation of TRPV1 Receptors by 1- and 2-Photon Excitation. *Biochemistry* 45, 4915–4926.
- (36) Carr, J. L., Wease, K. N., Van Ryssen, M. P., Paterson, S., Agate, B., Gallagher, K. A., Brown, C. T. A., Scott, R. H., and Conway, S. J.

- (2006) In vitro photo-release of a TRPV1 agonist. *Bioorg. Med. Chem. Lett.* 16, 208–212.
- (37) Van Ryssen, M. P., Avlonitis, N., Giniatullin, R., McDougall, C., Carr, J. L., Stanton-Humphreys, M. N., Borgstroem, E. L. A., Brown, C. T. A., Fayuk, D., Surin, A., Niittykoski, M., Khiroug, L., and Conway, S. J. (2009) Synthesis, photolysis studies and in vitro photorelease of caged TRPV1 agonists and antagonists. *Org. Biomol. Chem.* 7, 4695–4707.
- (38) Lu, M., Fedoryak, O. D., Moister, B. R., and Dore, T. M. (2003) Bhc-diol as a photolabile protecting group for aldehydes and ketones. *Org. Lett.* 5, 2119–2122.
- (39) Rea, A. C., Vandenberg, L. N., Ball, R. E., Snouffer, A. A., Hudson, A. G., Zhu, Y., McLain, D. E., Johnston, L. L., Lauderdale, J. D., Levin, M., and Dore, T. M. (2013) Light Activated Serotonin for Exploring Its Action in Biological Systems. *Chem. Biol.* 20, 1536–1546.
- (40) Abate-Pella, D., Zeliadt, N. A., Ochocki, J. D., Warmka, J. K., Dore, T. M., Blank, D. A., Wattenberg, E. V., and Distefano, M. D. (2012) Photochemical Modulation of Ras-Mediated Signal Transduction Using Caged Farnesyltransferase Inhibitors: Activation via One- and Two-Photon Excitation. *ChemBioChem* 13, 1009–1016.
- (41) Liu, Z., Liu, T., Lin, Q., Bao, C., and Zhu, L. (2014) Photoreleasable thiol chemistry for facile and efficient bioconjugation. *Chem. Commun.* 50, 1256–1258.
- (42) Mahmoodi, M. M., Fisher, S. A., Tam, R. Y., Goff, P. C., Anderson, R. B., Wissinger, J. E., Blank, D. A., Shoichet, M. S., and Distefano, M. D. (2016) 6-Bromo-7-hydroxy-3-methylcoumarin (mBhc) is an efficient multi-photon labile protecting group for thiol caging and three-dimensional chemical patterning. *Org. Biomol. Chem.* 14, 8289–8300.
- (43) Mahmoodi, M. M., Abate-Pella, D., Pundsack, T. J., Palsuledesai, C. C., Goff, P. C., Blank, D. A., and Distefano, M. D. (2016) Nitrodibenzofuran: A One- and Two-Photon Sensitive Protecting Group That Is Superior to Brominated Hydroxycoumarin for Thiol Caging in Peptides. *J. Am. Chem. Soc.* 138, 5848–5859.
- (44) Wong, P. T., Tang, S., Cannon, J., Mukherjee, J., Isham, D., Gam, K., Payne, M., Yanik, S. A., Baker, J. R., Jr., and Choi, S. K. (2017) A Thioacetal Photocage Designed for Dual Release: Application in the Quantitation of Therapeutic Release by Synchronous Reporter Decaging. *ChemBioChem* 18, 126–135.
- (45) Sun, S., Oliveira, B. L., Jimenez-Oses, G., and Bernardes, G. J. L. (2018) Radical-Mediated Thiol-Ene Strategy: Photoactivation of Thiol-Containing Drugs in Cancer Cells. *Angew. Chem., Int. Ed.* 57, 15832–15835.
- (46) Bader, T. K., Xu, F., Hodny, M. H., Blank, D. A., and Distefano, M. D. (2020) Methoxy-Substituted Nitrodibenzofuran-Based Protecting Group with an Improved Two-Photon Action Cross-Section for Thiol Protection in Solid Phase Peptide Synthesis. *J. Org. Chem.* 85, 1614–1625.
- (47) Zhu, Y., Pavlos, C. M., Toscano, J. P., and Dore, T. M. (2006) 8-Bromo-7-hydroxyquinoline as a Photoremovable Protecting Group for Physiological Use: Mechanism and Scope. *J. Am. Chem. Soc.* 128, 4267–4276.
- (48) Devos, M., Patte, F., Rouault, J., Laffort, P., and Van Gemert, L. J., (Eds.) (1990) *Standardized Human Olfactory Thresholds*; Oxford University Press, Oxford, UK.
- (49) Xu, H., Delling, M., Jun, J. C., and Clapham, D. E. (2006) Oregano, thyme and clove-derived flavors and skin sensitizers activate specific TRP channels. *Nat. Neurosci.* 9, 628–635.
- (50) Premkumar, L. S. (2014) Transient receptor potential channels as targets for phytochemicals. *ACS Chem. Neurosci.* 5, 1117–1130.
- (51) Bandell, M., Story, G. M., Hwang, S. W., Viswanath, V., Eid, S. R., Petrus, M. J., Earley, T. J., and Patapoutian, A. (2004) Noxious cold ion channel TRPA1 is activated by pungent compounds and bradykinin. *Neuron* 41, 849–857.
- (52) Macpherson, L. J., Geierstanger, B. H., Viswanath, V., Bandell, M., Eid, S. R., Hwang, S., and Patapoutian, A. (2005) The Pungency of Garlic: Activation of TRPA1 and TRPV1 in Response to Allicin. *Curr. Biol.* 15, 929–934.
- (53) Wang, G., Carey, A. F., Carlson, J. R., and Zwiebel, L. J. (2010) Molecular basis of odor coding in the malaria vector mosquito *Anopheles gambiae*. *Proc. Natl. Acad. Sci. U. S. A.* 107, 4418–4423.
- (54) Kajiya, K., Inaki, K., Tanaka, M., Haga, T., Kataoka, H., and Touhara, K. (2001) Molecular bases of odor discrimination: reconstitution of olfactory receptors that recognize overlapping sets of odorants. *J. Neurosci.* 21, 6018–6025.
- (55) Marchese, A., Barbieri, R., Coppo, E., Orhan, I. E., Daglia, M., Nabavi, S. F., Izadi, M., Abdollahi, M., Nabavi, S. M., and Ajami, M. (2017) Antimicrobial activity of eugenol and essential oils containing eugenol: A mechanistic viewpoint. *Crit. Rev. Microbiol.* 43, 668–689.
- (56) Barboza, J. N., Filho, C. d. S. M. B., Silva, R. O., Medeiros, J. V. R., and de Sousa, D. P. (2018) An overview on the anti-inflammatory potential and antioxidant profile of eugenol. *Oxid. Med. Cell. Longevity* 2018, 3957262.
- (57) Bobkov, Y. V., Corey, E. A., and Ache, B. W. (2011) The pore properties of human nociceptor channel TRPA1 evaluated in single channel recordings. *Biochim. Biophys. Acta, Biomembr.* 1808, 1120–1128.
- (58) Erythropel, H. C., Jabba, S. V., DeWinter, T. M., Mendizabal, M., Anastas, P. T., Jordt, S. E., and Zimmerman, J. B. (2019) Formation of flavorant-propylene Glycol Adducts With Novel Toxicological Properties in Chemically Unstable E-Cigarette Liquids. *Nicotine Tob. Res.* 21, 1248–1258.
- (59) Cao, E., Liao, M., Cheng, Y., and Julius, D. (2013) TRPV1 structures in distinct conformations reveal activation mechanisms. *Nature* 504, 113–118.
- (60) Liao, M., Cao, E., Julius, D., and Cheng, Y. (2013) Structure of the TRPV1 ion channel determined by electron cryo-microscopy. *Nature* 504, 107–112.
- (61) Gao, Y., Cao, E., Julius, D., and Cheng, Y. (2016) TRPV1 structures in nanodiscs reveal mechanisms of ligand and lipid action. *Nature* 534, 347–351.
- (62) Suo, Y., Wang, Z., Zubcevic, L., Hsu, A. L., He, Q., Borgnia, M. J., Ji, R.-R., and Lee, S.-Y. (2020) Structural Insights into Electrophile Irritant Sensing by the Human TRPA1 Channel. *Neuron* 105 (882), 882–894, DOI: 10.1016/j.neuron.2019.11.023.
- (63) Hinman, A., Chuang, H.-h., Bautista, D. M., and Julius, D. (2006) TRP channel activation by reversible covalent modification. *Proc. Natl. Acad. Sci. U. S. A.* 103, 19564–19568.
- (64) Talaga, A. K., Dong, F. N., Reisert, J., and Zhao, H. (2017) Cilia- and flagella-associated protein 69 regulates olfactory transduction kinetics in mice. *J. Neurosci.* 37, 5699–5710.
- (65) Nagashima, A., and Touhara, K. (2010) Enzymatic conversion of odorants in nasal mucus affects olfactory glomerular activation patterns and odor perception. *J. Neurosci.* 30, 16391–16398.
- (66) Hatchard, C. G., and Parker, C. A. (1956) A new sensitive chemical actinometer. II. Potassium ferrioxalate as a standard chemical actinometer. *Proc. R. Soc. London, Ser. A* 235, 518–536.
- (67) Furuta, T., Wang, S. S. H., Dantzer, J. L., Dore, T. M., Bybee, W. J., Callaway, E. M., Denk, W., and Tsien, R. Y. (1999) Brominated 7-hydroxycoumarin-4-ylmethyls: photolabile protecting groups with biologically useful cross-sections for two photon photolysis. *Proc. Natl. Acad. Sci. U. S. A.* 96, 1193–1200.
- (68) Paulsen, C. E., Armache, J.-P., Gao, Y., Cheng, Y., and Julius, D. (2015) Structure of the TRPA1 ion channel suggests regulatory mechanisms. *Nature* 520, 511–517.
- (69) Wang, Y. Y., Chang, R. B., Waters, H. N., McKemy, D. D., and Liman, E. R. (2008) The Nociceptor Ion Channel TRPA1 Is Potentiated and Inactivated by Permeating Calcium Ions. *J. Biol. Chem.* 283, 32691–32703.
- (70) Hill, K., and Schaefer, M. (2009) Ultraviolet light and photosensitising agents activate TRPA1 via generation of oxidative stress. *Cell Calcium* 45, 155–164.